Hindawi
Advances in Condensed Matter Physics
Volume 2023, Article ID 7808434, 11 pages
https://doi.org/10.1155/2023/7808434

Research Article

First-Principles Study of the Quasi-Particle and Excitonic Effect in o-BC_2N: The GW + BSE Study

Genene Shiferaw Aga,[1,2] **Pooran Singh**,[1] **and Chernet Amente Geffe**[1]

[1]*Department of Physics, College of Natural and Computational Sciences, Addis Ababa University, P.O. Box 1176, Addis Ababa, Ethiopia*
[2]*Department of Physics, College of Natural and Computational Sciences, Debre Birhan University, P.O. Box 445, Debre Birhan, Ethiopia*

Correspondence should be addressed to Genene Shiferaw Aga; genene235@gmail.com and Chernet Amente Geffe; chernet.amente@aau.edu.et

Received 7 September 2022; Revised 9 January 2023; Accepted 11 January 2023; Published 30 January 2023

Academic Editor: Sergio Ulloa

Ternary boron-carbon-nitride compounds are the hardest, chemically stable, and most applicable semiconductors in optoelectronic devices. We investigate the quasi-particle and excitonic properties of type II o-BC_2N using many-body perturbation theory (MBPT). The state-of-the-art GW and BSE methods were used to determine the accurate band gap and excited-state characteristics of this material. We simulate the convergence test and structural optimization in DFT, which is the starting point for the GW calculation. We also compute the convergence test of the parameters in GW and BSE. As a result, the bandgap of our system is found to be 2.31 eV and 1.95 eV using the GW approximation and DFT-PBE, respectively. Since the valence and conduction band edges are located at different Brillouin zones, we decide that o-BC_2N is an indirect bandgap semiconductor. In addition, by applying the scissor operator, we corrected the quasi-particle bandgap, which shows almost the same result as the GW approximation. Furthermore, using the BSE algorithm, we calculate the optical bandgap of type II o-BC_2N to be 4.0 eV with the excitonic effect and 4.4 eV without the excitonic effect. The highest peaks of the imaginary dielectric function with the excitonic effect shift to a lower energy level at 11 eV than without the excitonic effect at 13.5 eV. The electron charge distribution is computed by fixing the hole position. Finally, we suggest that type II o-BC_2N is promising for the application of optoelectronic semiconductors.

1. Introduction

Triplet, boron-carbon-nitrogen (B-C-N) substances have recently garnered significant interest since they represent a new type of higher strength material with exceptionally high hardness comparable to diamond [1–3] and outstanding thermochemical stability as cubic boron nitride (c-BN) [4]. Furthermore, B-C-N compounds are expected to operate for electrical and optoelectronic devices because their bandgaps are considered to be midway between semimetallic graphite and insulator hexagonal BN (hBN) and may be controlled by the atomic content and atomic structure [5, 6]. In addition to the normal characteristics, B-C-N materials may display a variety of other notable properties, including vibrational and thermal properties [7].

Diamond-like BC_2N (c-BC_2N) has received a lot of interest among triple B-C-N systems. Despite the fact that various purported cubic BC_2N compounds have been effectively produced [8, 9], the crystalline phase of BC_2N has yet to be confirmed definitively. As a result, the majority of theoretical and empirical investigations focused on BC_2N's structural forms and mechanical properties.

Numerous structures have already been proposed so far, such as zinc-blende [10], chalcopyrite [11], tetragonal [12], wurtzite [13], body-centered BC_2N [14], low-density [15], and type II or orthorhombic structures [16] of BC_2N.

Among these structures, the zinc-blende phase was assumed to be accurate due to its simulated X-ray diffraction (XRD) spectrum, which agreed well with the experimental data [12], and the tetragonal phase was predicted to be another candidate because the simulated XRD and Raman patterns agreed well with the experimental results.

Density functional theory (DFT) [17, 18] is a single-particle technique that is extremely successful in determining the ground-state electrical characteristics of many electron materials. The Kohn–Sham (KS) DFT formalism is widely used to understand and predict the structural, electronic, magnetic, and other properties of a wide range of molecules and condensed matter systems. When using the local density approximation (LDA) or generalized gradient approximation (GGA) functionals, depending on the KS energy levels (or bands) results in consistent 30–100% underestimation of the electronic bandgap (Egap) of semiconducting compounds and insulators [19].

This effect occurs to be independent of the nature of the system [20], and the bandgap's underestimation has been attributed to their inherent lack of derivative discontinuity [21, 22] and delocalization errors [23]. As a result, it is clear that precise prediction of bandgaps is one of the crucial problems in DFT, with potentially broad applications in many scientific fields such as photocatalytic processes and optoelectronic devices.

Semiempirical approaches, such as DFT + U [24–26] and hybrid density functionals (HSE) [27], which were originally developed to improve the description of the ground-state energies of small molecules, have been shown to improve the description of bandgaps in semiconductor systems [28]. Furthermore, the prediction of quasi-particles necessitates the use of many-body techniques, such as the many-body perturbation theory (MBPT) based on the GW method, to describe the energies of solid-state electronic excitation spectra. Despite its high computational cost, GW accurately predicts the quasiparticle energies of the materials [29].

The whole excitation spectrum of systems may be obtained by using time-dependent density functional theory (TDDFT) [30]. However, when common (semi) local functionals [31] are applied, they fail in most cases to reproduce charge-transfer excitations. These problems opened the way for the achievement of range-separated hybrid functionals [27, 32] that seem to be accurate for both local and charge-transfer excitations [33], despite the fact that transferability of variables influencing short and long-range exchange contributions [34, 35] is still a difficult problem.

Recently, another method derived from many-body perturbation theory (MBPT) within Green's function formalism, known as the GW approximation [36, 37] and the Bethe–Salpeter equation (BSE) [38] algorithm, which were originally developed for bulk semiconductors, has been successfully applied to the problem of charge-transfer excitations.

Moreover, the GW approach has lately become a widely used method for calculating bandgaps and charged excitation energies for extended [39, 40] and finite systems [29, 41]. Many-body perturbation theory (MBPT) [42] presents a natural framework for an ab initio, parameter-free explanation of photo-ionization processes and charged excitations [43] in the GW technique for electron self-energy [36, 44, 45]. Due to the electrostatic Coulomb interaction, an electron stimulated to a conduction band state in a semiconductor or an insulator may form a bonded state with the hole it leaves behind in the valence band state. The electrically neutral quasi-particle (QP), also known as an exciton [46], has a hydrogenic wave function with a much smaller binding energy and a much larger particle size than a hydrogen atom due to the relatively small effective masses of the excited electron and hole, as well as the screening of the Coulomb force by other electrons in the system. The attractive interaction between electrons and holes, which is commonly represented by the exciton binding energy, contributes to the creation of excitons [46], trions (charged excitons) [47, 48], and biexcitons [49].

In semiconductor-based optoelectronic devices, such as light-emitting diodes and laser diodes, the excitonic effect is essential [50–52]. Radiative recombination of excitons is thought to be far more efficient than that of free electrons and holes. Materials having packed and stable excitons are thus promising for low-threshold lasing.

In this study, we apply many-body perturbation theory (MBPT) methods, such as the GW approximation (GWA) in conjunction with the Bethe-Salpeter equation (BSE) formalism to calculate the quasi-particle bandgap and the characteristics of two body electron-hole bound states associated with neutral excitations of bulk type II o-BC_2N semiconductors. To the best of our knowledge, there is no scientific paper that shows the quasi-particle bandgap and the excitonic effect of type II o-BC_2N using GW and BSE. The convergence test for both GWA and BSE is computed carefully.

2. Computational Details

2.1. Ground-State Calculations. The DFT calculation was performed with the Quantum ESPRESSO software [53, 54]. The generalized gradient approximation (GGA) with the Perdew–Burke–Ernzerhof (PBE) [55, 56] functional describes the exchange correlation. We employ the norm-conserving Vanderbilt pseudopotential [57], as used in electron-ion interactions. We expanded the one-electron wave functions on a plane-wave basis, with the plane-wave energy cutoff set at 544 eV to assure total energy convergence to 0.001 eV per primitive cell. The Broyden–Fletcher–Goldfarb–Shanno (BFGS) [58] method was used for structural optimization. The ground-state convergence threshold is set at 10^8 eV between two subsequent simulation steps, and all atoms may be completely relaxed throughout geometric optimization till the Hellmann–Feynman force acting on each atom is less than 0.01 eV. The many-body effect is realized within the GWA by employing ground-state Kohn–Sham (KS) wave functions and corresponding eigenvalues (G0W0) [59].

The convergence criteria were set at 3.6×10^9 Ry/cell in energy and 0.4 for mixing. Following relaxation, the Brillouin zone (BZ) was integrated using a $7 \times 7 \times 7k$-point grid. Our model began with a DFT calculation for the plane-wave self-consistent field and then continued to crystal structure

optimization. We utilized this result as input for the Yambo code by applying the command p2y, and then, the excitation-state calculation was performed.

2.2. Excited-State Calculation: Bandgap Correction and Optical Properties. Electronic excitations are not sufficiently described by fundamental KS theory since DFT calculates the ground state, and quasi-particle (QP) effects must be incorporated. A well-known disadvantage of DFT is the underestimation of the bandgap. To circumvent this problem, we employed the cutting-edge GWA, which works very well for calculating the bandgap in most semiconductors.

The Yambo code [60, 61] was used to compute QP adjustments at G0W0 and self-consistent GW (evGW), which were then utilized for BSE computations. The plasmon-pole approximation (PPA) [62, 63] was used to calculate the inverse dielectric matrix for the GWA. After we computed the convergence test of the parameters, we set the following parameters as the starting point for our calculation. A 40 Ry energy cutoff for the exchange component of self-energy (the number of G-vectors in the exchange), a 4 Ry cutoff for the correlation part (energy cutoff in the screening) or response block size, 30 bands in the independent response function, 30 GW bands to expand Green's function, and Newton linearization are used to calculate the GWA. In addition, the fourth round of GW self-consistency on eigenvalue alone (evGW) was utilized.

The BSE computation was performed after the GW calculation, and evGW was utilized throughout the BSE calculation. The convergence test of the parameters in the BSE calculation is also essential. Once we test their convergency, we decided to use a 4 Ry cutoff energy (screened interaction (W) or electron-hole interaction), 30 Ry Hartree potential (V) components, 4–12 Bethe–salpeter (BS) bands (5 occupied and 4 unoccupied states), a diagonalization solver (calculates all exciton energies and composition in terms of electron-hole pair) for BSE, and a $12\times12\times4$ k-point mesh for both GW and BSE calculations.

3. Mathematical Formulation

The mathematical derivation of the GW and BSE calculation is as follows. We start from the generalized gradient approximation of the Kohn–Sham (KS) equation, which is given as

$$\left[-\frac{1}{2}\nabla^2 + V_{eff}(\mathbf{r})\right]\varphi_{n\mathbf{k}}^{KS}(\mathbf{r}) = E_{n\mathbf{k}}^{KS}\varphi_{n\mathbf{k}}^{KS}(\mathbf{r}), \tag{1}$$

where $V_{\text{eff}} = V_{\text{ext}}(\mathbf{r}) + V_H(\mathbf{r}) + V_{xc}(\mathbf{r})$, ∇^2 is the kinetic energy, V_{ext} is the external potential, V_H is the Hartree potential, and V_{xc} is the exchange-correlation potential.

The perturbatively corrected GW QP eigenvalues are obtained by replacing the exchange-correlation contribution to the KS eigenvalues (Equation (1)) with $\sum_{xc}(\mathbf{r}, \mathbf{r}', E)$ self-energy (calculated by the GWA) that accounts for many-body exchange-correlation effects. As a result, Equation (1) can be rewritten as

$$\left[-\frac{1}{2}\nabla^2 + V_{ext}(\mathbf{r}) + V_H(\mathbf{r}) + \int\sum_{xc}\left(\mathbf{r}, \mathbf{r}'; E_{n\mathbf{k}}^{qp}\right)]\varphi_i^{qp}(\mathbf{r}')d\mathbf{r}' = E_{n\mathbf{k}}^{qp}\varphi_{n\mathbf{k}}^{qp}(\mathbf{r}), \tag{2}$$

where $\sum_{xc}(\mathbf{r}, \mathbf{r}'; E_{n\mathbf{k}}^{qp})$ is the energy-dependent self-energy operator.

The quasi-particle (QP) energy with the GW approximation is given by

$$E_{n\mathbf{k}}^{qp} = E_{n\mathbf{k}}^{KS} + M_{n\mathbf{k}}\left[Re\sum_{n\mathbf{k}}\left(E_{n\mathbf{k}}^{KS}\right) - V_{n\mathbf{k}}^{xc}\right], \tag{3}$$

where $E_{n\mathbf{k}}^{KS}$ is the KS eigenvalue, $\Sigma_{n\mathbf{k}}$ and $V_{n\mathbf{k}}^{xc}$ are the diagonal matrix elements of self-energy and the exchange-correlation (xc) potential that is employed in the single-particle KS Hamiltonian. The QP renormalization factor $M_{n\mathbf{k}}$ accounts for the energy dependence of self-energy and is given by

$$M_{n\mathbf{k}} = \left[1 - \frac{\mathrm{d}\sum_{n\mathbf{k}}(\omega)}{\mathrm{d}\omega}\Big|_{\omega=E_{n\mathbf{k}}^{KS}}\right]^{-1}. \tag{4}$$

For $M_{n\mathbf{k}} \ll 1$, we may deduce that $\varphi_{n\mathbf{k}}^{KS}$ is not a (correct) QP state. The two possible explanations for this are as follows: The first explanation is that electrons are tightly correlated, and hence, the QP image does not apply; the second one is that $\varphi_{n\mathbf{k}}^{KS}$ is a poor approximation to the genuine QP wave function $\varphi_{n\mathbf{k}}^{qp}$. While the former argument is based on the physics of the underlying electron system, the latter argument simply states that the Kohn–Sham orbital does not adequately reflect actual many-body excitations. For instance, where the QP image is totally correct, that is, all QP states have norms extremely near to 1 or 0, yet simple noninteracting orbitals do not offer a decent approximation to them [64].

The self-energy operator in Equation (2) includes all interactions beyond the Hartree contribution given by

$$\sum_{xc}\left(\mathbf{r}, \mathbf{r}'; E_{n\mathbf{k}}^{qp}\right) = iGW, \sum_{xc}\left(\mathbf{r}, \mathbf{r}'; E_{n\mathbf{k}}^{qp}\right) = \frac{i}{2\pi}\int G\left(\mathbf{r}, \mathbf{r}'; E_{n\mathbf{k}}^{qp} + \omega\right)W(\mathbf{r}, \mathbf{r}'; \omega)\exp^{i\omega\vartheta}\mathrm{d}\omega, \tag{5}$$

where G is Green's function and W is dynamically screened Coulomb potential and are given as

$$G\left(\mathbf{r},\mathbf{r}';E_{n\mathbf{k}}^{qp}+\omega\right)=\sum_{n}\sum\frac{\varphi_n(\mathbf{r})\varphi_n^*(\mathbf{r}')}{E_{n\mathbf{k}}^{qp}-\varepsilon_n+\vartheta sgn\left(\varepsilon_n-E_F\right)},W(\mathbf{r},\mathbf{r}';\omega)=\int\varepsilon^{-1}(\mathbf{r},\mathbf{r}'';\omega)V(\mathbf{r}',\mathbf{r}'')\mathrm{d}\mathbf{r}''. \tag{6}$$

φ_n and ε_n are the input single-particle eigenstates/eigenenergies derived from DFT Kohn–Sham computations, respectively. The Fermi level is denoted by E_F, while the bare Coulomb potential is denoted by V in the KS calculation. The inverse dynamical dielectric matrix, ε^{-1}, is derived below inside the random-phase approximation, and χ_o is the independent-electron susceptibility. To ensure convergence, the infinitesimally tiny positive value (ϑ) is added while performing a Fourier transformation from time to frequency space.

The microscopic inverse dielectric function in the reciprocal vector is given by [36, 37]

$$\varepsilon_{\mathbf{G},\mathbf{G}'}^{-1}(\mathbf{q},\omega)=\delta_{\mathbf{G},\mathbf{G}'}+V_{\mathbf{G}}(q)\chi_{\mathbf{G},\mathbf{G}'}(\mathbf{q},\omega), \tag{7}$$

where the bare Coulomb interaction in a reciprocal vector is

$$V_{\mathbf{G}}(\mathbf{q})=\frac{4\pi}{|\mathbf{q}+\mathbf{G}||\mathbf{q}+\mathbf{G}'|}. \tag{8}$$

The polarization susceptibility $\chi_{\mathbf{G},\mathbf{G}'}(\mathbf{q},\omega)$ is given by

$$\chi_{\mathbf{G},\mathbf{G}'}(\mathbf{q},\omega)=\chi_{\mathbf{G},\mathbf{G}'}^{o}(\mathbf{q},\omega)+\sum_{\mathbf{G}_1,\mathbf{G}_2}\chi_{\mathbf{G},\mathbf{G}_1}(\mathbf{q},\omega)\left[V_{\mathbf{G}_1}(\mathbf{q})\delta_{\mathbf{G}_1\mathbf{G}_2}+f_{\mathbf{G}_1\mathbf{G}_2}^{xc}\right]\chi_{\mathbf{G}_2,\mathbf{G}'}(\mathbf{q},\omega), \tag{9}$$

where $f_{\mathbf{G}_1\mathbf{G}_2}^{xc}$ is the xc kernel that accounts for the exchange and correlation effects.

In PPA, the frequency dependence of the dielectric function $\varepsilon_{\mathbf{G},\mathbf{G}'}^{-1}(\mathbf{q},\omega)$ is modeled as a single-pole approximation:

$$\varepsilon_{\mathbf{G},\mathbf{G}'}^{-1}(\mathbf{q},\omega)=R_{\mathbf{GG}}(\mathbf{q})\left(\frac{1}{\omega-\omega_{\mathbf{G},\mathbf{G}'}(\mathbf{q})+i\vartheta}-\frac{1}{\omega+\omega_{\mathbf{G},\mathbf{G}}(\mathbf{q})-i\vartheta}\right), \tag{10}$$

where $\omega_{\mathbf{G},\mathbf{G}'}$ and $R_{\mathbf{G},\mathbf{G}'}(\mathbf{q})$ are the plasmon frequency and the real spectral function, respectively.

For optical calculations, we employed a variety of approximations, including the independent-particle approximation with local-field effects and the Bethe–Salpeter equation.

Before delving into the data, we will go through the theoretical approximations that have been utilized to compute optical absorption. The optical spectra are derived at the level of the Bethe–Salpeter equation (BSE) starting from the Kohn–Sham wave functions and quasi-particles [65–68]:

$$\left(E_{c\mathbf{k}}^{qp}-E_{v\mathbf{k}}^{qp}\right)B_{vc\mathbf{k}}^{S}+\sum_{\mathbf{k}'c'}\langle vc\mathbf{k}|\kappa_{eh}|v'c'\mathbf{k}'\rangle B_{v'c'\mathbf{k}'}^{S}=\Omega^{S}B_{vc\mathbf{k}}^{S}, \tag{11}$$

where $B_{vc\mathbf{k}}^{S}$ and Ω^{S} are the excited eigenstates and eigenvalues (energy of excited states) for the S^{th} exciton. Electronic excitations are represented in terms of electron-hole pairs (i.e., vertical excitations at a particular k-point from a valence band state (v) with quasi-particle energy $E_{v\mathbf{k}}^{qp}$ to a conduction band state (c) with energy $E_{c\mathbf{k}}^{qp}$). The interaction kernel κ_{eh} defines the screened Coulomb interaction between electrons and holes as well as the exchange interaction, which includes local-field effects.

In this framework, the electron-hole amplitude in the real space (or the wave function of excitons) is given by the Tamm–Dancoff approximation as follows [66, 69–71]:

$$\Phi_S(\mathbf{r}_e,\mathbf{r}_h)=\sum_{k}\sum_{v}\sum_{c}B_{vc\mathbf{k}}^{S}\phi_{c\mathbf{k}}(\mathbf{r}_e)\phi_{v\mathbf{k}}^{*}(\mathbf{r}_h), \tag{12}$$

where $\phi_{c\mathbf{k}}(\mathbf{r}_e)$ and $\phi_{v\mathbf{k}}^{*}(\mathbf{r}_h)$ are the wave function of the electron in the conduction band and hole in the valence band at the wave vector $\mathbf{k}$ in the real space.

The exciton state is represented by the expansion of the following equation [72]:

$$|S\rangle=\sum_{\mathbf{k}}\sum_{v}^{h}\sum_{c}^{e}B_{vc\mathbf{k}}^{S}|vc\mathbf{k}\rangle. \tag{13}$$

If the interaction kernel κ_{eh} is missing, Equation (11) merely returns $\Omega^{S}=E_{c\mathbf{k}}^{qp}-E_{v\mathbf{k}}^{qp}$, indicating that the system's excitations belong to separate electron-hole pairs.

The imaginary portion of the dielectric function (ε_2) gives the optical absorption spectrum, which may be computed as [68]

$$\epsilon_2(\hbar\omega)\propto\sum_{S}\left|\sum_{cv\mathbf{k}}B_{vc\mathbf{k}}^{S}\frac{\langle c\mathbf{k}|\eta|v\mathbf{k}\rangle|}{E_{c\mathbf{k}}-E_{v\mathbf{k}}}\right|\delta\left(\Omega^{S}-\hbar\omega-\gamma\right), \tag{14}$$

where the dipole matrix elements for electronic transitions from valence to conduction states are $\langle c\mathbf{k}|\eta|v\mathbf{k}\rangle$ and γ is widening of energy. We only examine light absorption with polarization, and hence, the orientation of the dipole operator η is obtained.

4. Results and Discussion

4.1. Parameter Optimization and Structural Stability. We model primitive unit cells of type II orthorhombic BC_2N. Then, we compute the convergence test with respect to the plane-wave kinetic energy cutoff and the k-point grid density using Quantum ESPRESSO. Because bad convergence tests usually result in an inaccurate converged total energy, these parameters are the primary starting points for any plane-wave self-consistent field (PWSCF) computations. The

convergence test calculation demonstrates that changes in the energy cutoff and k-points become stable at 544 eV and $7 \times 7 \times 7$, respectively. Hence, raising the energy cutoff above 544 eV and k-points above $7 \times 7 \times 7$ has no significant influence on total energy.

The optimization of the type II o-BC_2N crystal structure was calculated by considering the above convergence test. As a result, we found that the bond lengths of C-C, C-N, and C-B are 1.52, 1.56, and 1.58 Å, respectively. We also obtain the lattice constants $a = 2.52$, $b = 2.549$, and $c = 3.62$ Å, which are in good agreement with the earlier theoretical values of 2.527 Å, 2.533 Å, and 3.605 Å [11, 16]. Figures 1(a)–1(c) show the optimized crystal structure of type II o-BC_2N in $2 \times 2 \times 3$ supercells (see Figure 1(a)) and primitive unit cells (Figures 1(b)) and 1(c)) with space group Pmm2. The green, brown, and light blue colors correspond to boron, carbon, and nitrogen atoms, as depicted in the figure, respectively.

To confirm the structural stability of orthorhombic BC_2N (o-BC_2N), we computed phonon dispersion and found that this system is stable.

4.2. Electronic Properties. There are different computational methods to calculate the electrical properties of materials. Among these, DFT(GGA) is a computational method to evaluate the bandgap of the system, even though it has inaccuracy with respect to the experimental results. For a more accurate calculation of the quasi-particle bandgap, we apply the GW approximation. Before the calculation of the band structure of type II o-BC_2N, we compute the self-consistency test of GW on eigenvalues. This is because one-shot GW (G0W0) is insufficient to determine the accurate bandgap of the system. The importance of self-consistency by upgrading the eigenenergies of both G and W has been proved to be critical for many semiconductors in minimizing the effect of the starting point dependency on G0W0 [73]. To do this, we utilize the Yambo code, and our results are discussed as follows.

4.2.1. Self-Consistency of GW Eigenvalue Only and the Quasi-Particle Band Structure of Type II o-BC_2N. The G0W0 technique frequently produces unsatisfactory results for molecular systems and many solids. The main reason for this failure is that the DFT-starting point with local or semilocal exchange and correlation functionals results in an insufficiently small gap when compared to the experimental one, and a single-shot GW cannot compensate for this inaccuracy. This method has been used successfully to improve the G0W0 bandwidths and bandgaps of a wide range of solid materials [73]. This self-consistency of GW is calculated up to four iterations until the difference between consistent GW is 0.01 eV. We used up to four iterations because the bandgap is converged at this point, which means that taking above this level does not change the result of the bandgap; instead, it increases our computational cost, as shown in Figure 2(a)). There are several levels of the GW approach to enhance consistency with experiments. According to [74], partial self-consistency on Green's function G alone (GW0) and both G and the screened Coulomb interaction W (GW) can also widen the bandgap.

We determine the self-consistency of GW on eigenvalues only (evGW) as follows: First, from DFT, the KS eigenvalues and eigenstates are used in the first GW iterations to compute the expectation value of self-energy. Then, multiple GW iterations are performed, replacing the KS eigenvalues with the most recent GW QP values while leaving the KS eigenstates fixed. This technique is repeated until the GW gap is converged. Based on this result, QP energies and KS eigenvectors are then utilized to construct the BSE electron-hole Hamiltonian for the simulation of excitonic effects. In our case, Figure 2(a)) depicts the convergence test for four iterations of an evGW computation. Taking the fourth iteration into consideration, the quasi-particle HOMO-LUMO gap opened from the DFT-PBE calculation to the GW calculation.

We investigate the quasi-particle band structure of type II orthorhombic BC_2N (o-BC_2N) taking evGW into consideration. The band structure was computed along the path Γ (0.0, 0.0, 0.0) – X (0.5, 0.0, 0.0, 0.0) – S (0.5, 0.5, 0.0) – Y (0.0, 0.5, 0.0) – Γ (0.0, 0.0, 0.0) – Z (0.0, 0.0, 0.5) – U (0.5, 0.0, 0.5) – R (0.5, 0.5, 0.5) – T (0.0, 0.5, 0.5) – Z (0.0, 0.0, 0.5) at the Brillouin zone, which are high-symmetric points of the orthorhombic unit cell, as shown in Figure 2(b)), and the Fermi level is adjusted to zero. The results show that o-BC_2N possesses semiconductor qualities with a bandgap of 1.95 eV, 1.97 eV, and 2.31 eV applying DFT-PBE, G0W0, and evGW (G4W4), respectively. The top of the valence band and bottom of the conduction band are positioned in different locations, suggesting that type II o-BC_2N belongs to the indirect bandgap family. As we can observe from Figure 2(b)), the evGW (G4W4) correction shifts the valence band down and the conduction band up. First-principles calculations are performed by other academics accord well with our findings. Mattesini and Matar, for example, observed an indirect bandgap of 1.69 eV for type II o-BC_2N by employing LDA [16], and Bao et al. calculated 1.734 eV using GGA-PW91 [75], demonstrating the trustworthiness of our computational technique, since LDA is very poor in determining the bandgap of the system.

In addition, to correct the quasi-particle bandgap, we apply the scissor operator and renormalize the conduction and/or valence band, as shown in Figure 3. The impact of GW self-energy is an opening of the gap and a linear stretching of conduction/valence bands, which may be approximated by performing a linear fit of positive and negative energies (the zero is set at the top of the valence band). Hence, we found approximately the same result as that of GW QP calculation.

4.3. Optical Properties: Excitonic Effect. When a valence electron crosses a bandgap to the conduction band, it does not always escape the hole it creates. In some materials, Coulomb forces are strong enough to keep negatively charged electrons and positively charged holes together in neutral electron-hole pairs known as excitons. The existence and behavior of this quasi-particle influence the electrical

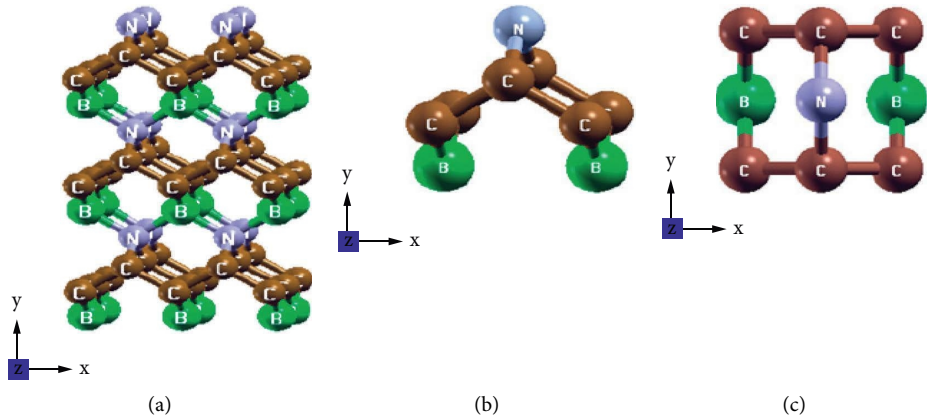

Figure 1: Optimized crystal structure of type II orthorhombic BC_2N: (a) supercells of o-BC_2N of $22 \times 2 \times 3$, (b) a side view of unit cells of o-BC_2N, and (c) a top view of unit cell crystal structures of o-BC2N, with the green color representing boron (B), the brown color representing carbon (C), and the light blue color representing nitrogen (N).

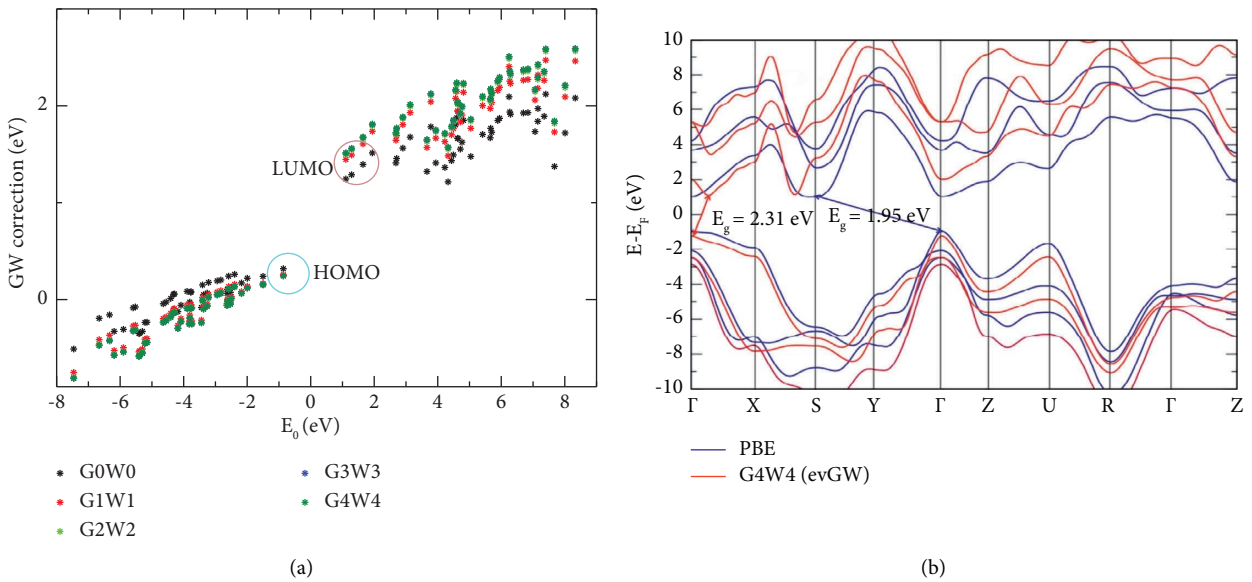

Figure 2: Quasi-particle bandgap calculation: (a) the convergence test of self-consistent GW on eigenvalues only for four iterations and (b) QP band structure calculation using evGW and DFT (PBE) methods.

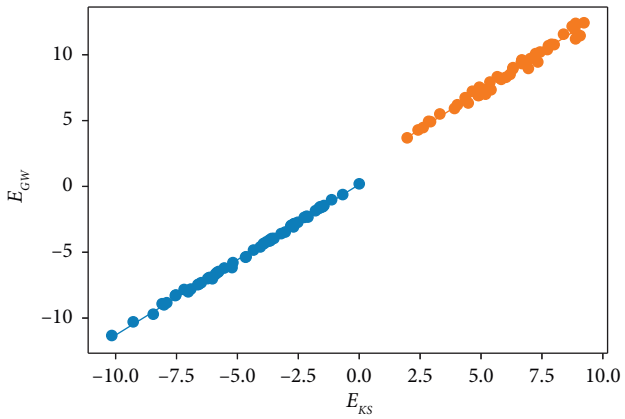

Figure 3: Scissor operator correction in QP and renormalization of conduction and valence bands. E_{GW} and E_{KS} are in electron volt (eV).

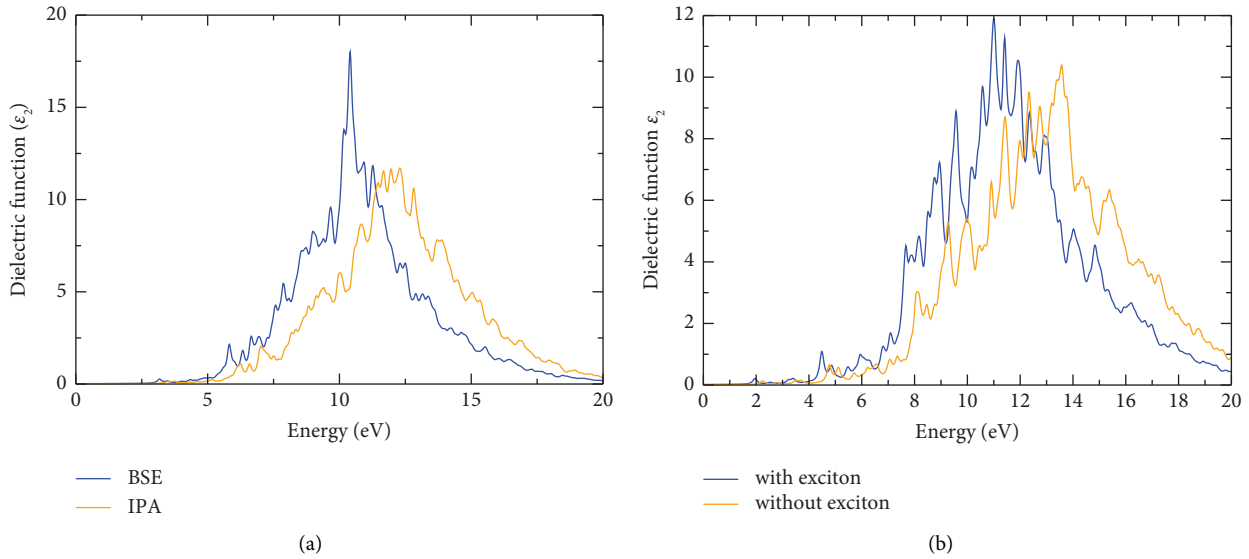

FIGURE 4: Optical spectra of imaginary dielectric function with arbitrary units: (a) the BSE and IPA result with respect to photon energy and (b) the excitonic effect in o-BC_2N using the BSE algorithm in the polarization direction *xyz* (/or (111)).

and optoelectronic properties of materials in which they reside.

The optical spectra of type II o-BC_2N are computed using the BSE algorithm based on our previous evGW (G4W4) result. Figure 4(a)) shows the calculated spectra of o-BC_2N with comparison of the BSE and independent particle approximation (IPA). The threshold frequency, commonly known as the optical gap, shifts to the lower energy for BSE than for IPA. The highest peaks were found at 10.2 eV and 11 eV for BSE and IPA, respectively. In addition to the threshold frequency, there are multiple nonvanishing and/or noticeable peaks. Cutting-edge analysis of concise physical and chemical representations in the atom-dominated bandgap, atom-orbital singularities, and strong optical responses are used to realize the optical excitation process. Figure 4(b) clearly shows the excitonic effect in type II o-BC_2N. We can exhibit the band edge optical spectrum of 4.0 eV and 4.4 eV with exciton (electron-hole interaction) and without excitonic effects, respectively. Furthermore, the predicted complex dielectric function ($\epsilon_2(\omega)$) has two main peaks with the exciton effect and without the excitonic effect, which are positioned at 11 eV and 13.5 eV, respectively. Due to its broad bandgap, the light response range of o-BC_2N with and without excitonic effects is restricted to the ultraviolet area, limiting solar energy usage.

Figure 5 depicts the absorption spectra of type II o-BC_2N by computing BSE and the renormalized (valence and conduction band) scissor operator. This makes a difference in peak positions, distribution, and intensity. Besides a simple shift, we renormalized the bandwidth of the valence and conduction bands. As a result, we found that opening the QP bandgap using a scissor operator shows a red shift with a high peak at 10 eV.

Figure 6 shows the amplitude and the strength of excitons of o-BC_2N. The strength of bright excitons is at 1, as

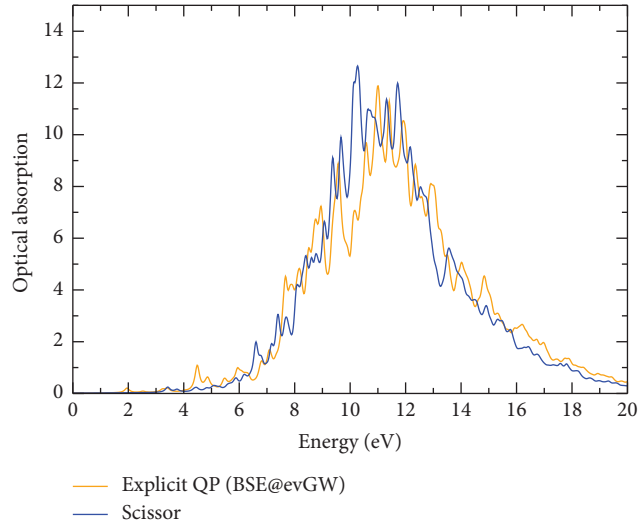

FIGURE 5: The absorption (arbitrary unit) of type II o-BC_2N using the BSE and scissor operator after renormalization of the valence band and conduction band in the polarization direction *xyz* (/or (111)).

shown in Figure 6(b), which is related to the highest peak shown in Figure 4(b), with (blue) excitonic effects.

The contribution of valence and conduction band states for the exciton is shown in Figure 7. The measured optical gap is composed of the transitions at the Γ point, as shown in Figure 7, which is corresponding to the strongest peak of ε_2 in Figure 4(b), as a result of the excitonic effect.

In the absence of exciton-phonon coupling, photon emission or absorption entails excited states $\Phi^S q$ (Equation (12)) of the total wave vector q corresponding to photon momentum, which is henceforth represented as $\mathbf{q} = 0$. To address the exciton localization for o-BC_2N, we compute the exciton probability $|\Phi^S(r_h, r_e)|^2$ for a given

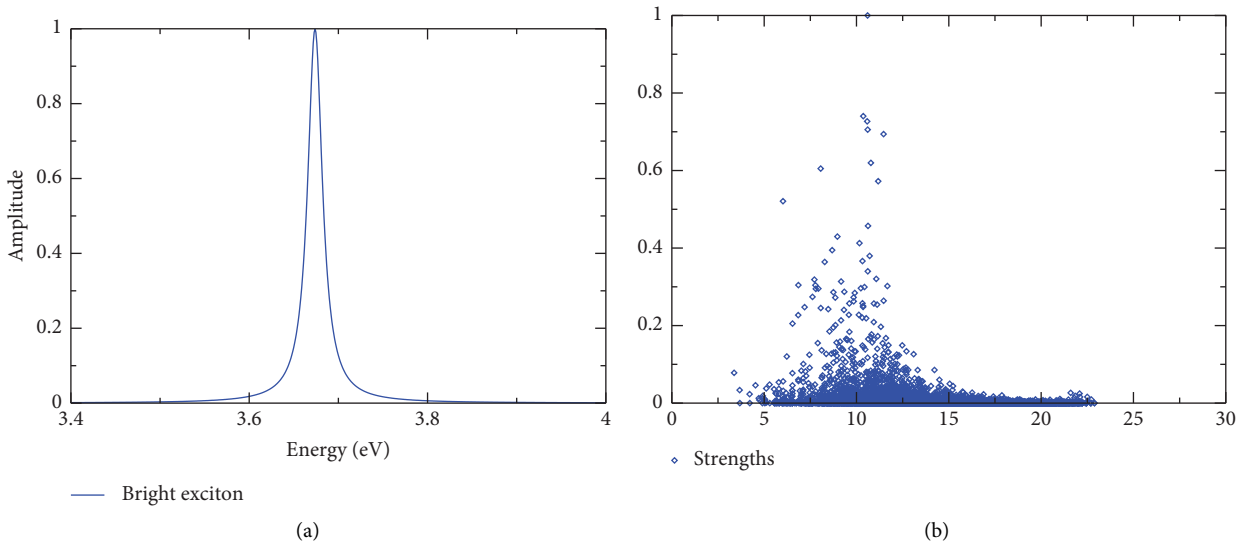

Figure 6: Exciton amplitude (a) and its strength (b) of the bright exciton.

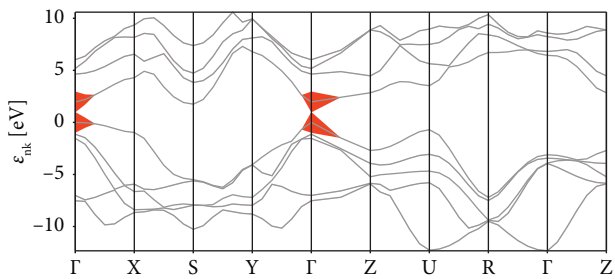

Figure 7: The contribution of the exciton at the valence band and conduction band edge.

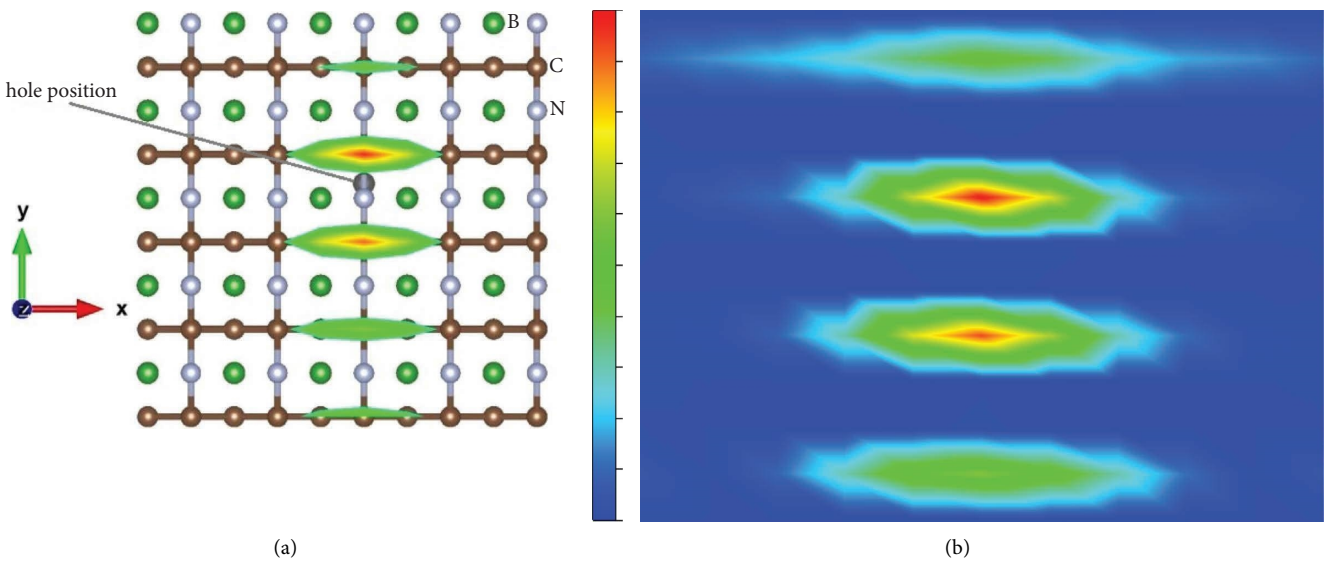

Figure 8: Exciton spatial distribution as the hole position fixed: (a) a top view of $5 \times 5 \times 1$ supercells of o-BC_2N with the green color representing boron (B), the brown color representing carbon (C), and light blue representing nitrogen (N) and (b) a two-dimensional contour plot of the probability density of finding electrons.

hole position $\mathbf{r}_h$ and illustrate the electron distribution relative to the hole for the excited state at 11 eV. Such a distribution is shown in Figure 8 for a hole located just above a nitrogen atom. The electron is delocalized on nitrogen atoms, as shown in Figure 8(a), and the likelihood of locating the electron on a nitrogen atom is

greatest for the boron atom's nearest neighbors where the hole is localized.

Similarly, in Figure 8(b), we calculate the exciton wave function, representing the electronic charge distribution $|\Phi^S(\mathbf{r}_h, \mathbf{r}_e)|^2$ for a fixed position of the hole $\mathbf{r}_h$, for the lowest energy exciton in the o-BC_2N system, which is visible for light polarized along the (111) axis. In accordance with earlier BSE computations [76, 77], we discover a charge-transfer exciton in o-BC_2N: the electronic charge is mostly concentrated on the nearest neighbor atoms with regard to the location of the hole. The charge-transfer nature of the exciton in o-BC_2N is caused by the interaction of the exchange electron-hole interaction with band dispersion, which causes the hopping term to be big enough to induce substantial mixing between Frankel and charge-transfer states.

When a single photon is absorbed, it produces a bright exciton. In the case of dark excitons, electrons and holes are connected by an optically forbidden transition, implying that the electron did not reach the conduction band only by photon absorption, which also required phonon scattering. Dark excitons are challenging to investigate using conventional optical methods because they can generate or recombine via a variety of paths.

5. Conclusion

In conclusion, we predicted the quasi-particle bandgap and the excitonic effect in type II orthorhombic BC_2N (o-BC_2N). To investigate the electronic and optical properties of this system, we performed the convergence test and structure optimization using state-of-the-art DFT and GW-BSE. We also calculate the self-consistent GW eigenvalue alone (evGW) for a better prediction of the quasi-particle bandgap, since the one-shot GW (G0W0) approximation is insufficient to approximate an accurate bandgap. Then, afterward, using DFT-PBE and GWA (evGW), we computed the quasi-particle bandgap and found that o-BC_2N has an indirect bandgap of 1.95 eV and 2.31 eV, respectively. This shows that the GWA has a better approximate bandgap than PBE. This disparity is due to the DFT-well-known PBE's flaw of underestimating the bandgap. In addition, we tried to correct the quasi-particle bandgap using the scissor operator, which shows almost the same result as the GW approximation. The valence band maximum (or HOMO) and conduction band minimum (or LUMO) are found at different Brillouin zones, and as a result, o-BC_2N is an indirect bandgap semiconductor. Furthermore, we calculated the optical properties of type II o-BC_2N with and without the electron-hole interaction (exciton). As a result, we observed the impact of the exciton, which changes the material properties from its bare (without exciton) o-BC_2N. According to the computed complex part of the dielectric function, the highest peaks occur at 11 eV and 13.5 eV with and/or without excitonic effects, respectively. This demonstrates that the dielectric function with excitons exhibits the optical spectrum shifts to lower photon energy than without the exciton effect. The highest peak in the presence of excitons also describes the strength of excitons. In the absence of exciton-phonon coupling, we calculated the electronic charge distribution by fixing the hole position. By establishing the position of the hole on the top of the *N* atom, we calculate the spatial distribution of the wave function of the electron in the real space. These findings recommend that o-BC_2N is a promising material for advanced applications in optoelectronic devices.

Data Availability

All data that support the findings of this study are included within the article.

Conflicts of Interest

The authors declare that they have no conflicts of interest.

Acknowledgments

The authors gratefully acknowledge Debre Birhan University for its support and the MOSHE (Ministry of Science and Higher Education) for the use of HPC computers.

References

[1] A. Y. Liu and M. L. Cohen, "Prediction of new low compressibility solids," *Science*, vol. 245, no. 4920, pp. 841-842, 1989.

[2] D. M. Teter and R. J. Hemley, "Low-compressibility carbon nitrides," *Science*, vol. 271, no. 5245, pp. 53–55, 1996.

[3] P. R. Møller, J. G. Nielsen, and I. Fossen, "Patagonian toothfish found off Greenland," *Nature*, vol. 421, no. 6923, p. 599, 2003.

[4] D. M. Teter, "Computational alchemy: the search for new superhard materials," *MRS Bulletin*, vol. 23, no. 1, pp. 22–27, 1998.

[5] X. D. Bai, E. G. Wang, J. Yu, and H. Yang, "Blue-violet photoluminescence from large-scale highly aligned boron carbonitride nanofibers," *Applied Physics Letters*, vol. 77, no. 1, pp. 67–69, 2000.

[6] T. Sugino and H. Hieda, "Field emission characteristics of boron carbon nitride films synthesized by plasma-assisted chemical vapor deposition," *Diamond and Related Materials*, vol. 9, no. 3-6, pp. 1233–1237, 2000.

[7] M. C. Polo, E. Martínez, J. Esteve, and J. L. Andújar, "Micromechanical properties of BN and B-C-N coatings obtained by r.f. plasma-assisted CVD," *Diamond and Related Materials*, vol. 8, no. 2-5, pp. 423–427, 1999.

[8] V. L. Solozhenko, D. Andrault, G. Fiquet, M. Mezouar, and D. C. Rubie, "Synthesis of superhard cubic BC2N," *Applied Physics Letters*, vol. 78, no. 10, pp. 1385–1387, 2001.

[9] Y. Gao, Y. Wu, Q. Huang et al., "Superhard sp 2- sp 3 hybridized BC2N: a 3D crystal with 1D and 2D alternate metallicity," *Journal of Applied Physics*, vol. 121, no. 22, Article ID 225103, 2017.

[10] X. F. Zhou, J. Sun, Q. R. Qian et al., "A tetragonal phase of superhard BC2 N," *Journal of Applied Physics*, vol. 105, no. 9, Article ID 093521, 2009.

[11] J. Sun, X. F. Zhou, G. R. Qian et al., "Chalcopyrite polymorph for superhard BC2N," *Applied Physics Letters*, vol. 89, no. 15, pp. 151911–151914, 2006.

[12] X. F. Zhou, J. Sun, Y. X. Fan et al., "Most likely phase of superhardBC2Nby*ab initio*calculations," *Physical Review B*, vol. 76, no. 10, pp. 100101–100104, 2007.

[13] X. Luo, X. Guo, Z. Liu et al., "First-principles study of wurtziteBC2N," *Physical Review B*, vol. 76, no. 9, pp. 092107–92114, 2007.

[14] X. Luo, X. Guo, B. Xu et al., "Body-centered superhardBC2Nphases from first principles," *Physical Review B*, vol. 76, no. 9, pp. 094103–094106, 2007.

[15] E. Kim, T. Pang, W. Utsumi, V. L. Solozhenko, and Y. Zhao, "Cubic phases ofBC2N: a first-principles study," *Physical Review B*, vol. 75, no. 18, pp. 184115–184117, 2007.

[16] M. Mattesini and S. F. Matar, "Search for ultra-hard materials: theoretical characterisation of novel orthorhombic BC2N crystals," *International Journal of Inorganic Materials*, vol. 3, no. 7, pp. 943–957, 2001.

[17] C. H. Chu and C. W. Leung, "The convolution equation of Choquet and Deny on [IN]-groups," *Integral Equations and Operator Theory*, vol. 40, no. 4, pp. 391–402, 2001.

[18] J. Y. Jung, J. H. Park, Y. J. Jeong et al., "Involvement of Bcl-2 family and caspases cascade in sodium fluoride-induced apoptosis of human gingival fibroblasts," *Korean Journal of Physiology and Pharmacology*, vol. 10, no. 5, pp. 289–295, 2006.

[19] J. P. Perdew and M. Levy, "Physical content of the exact Kohn-Sham orbital energies: band gaps and derivative discontinuities," *Physical Review Letters*, vol. 51, no. 20, pp. 1884–1887, 1983.

[20] A. D. Becke, "Perspective: fifty years of density-functional theory in chemical physics," *The Journal of Chemical Physics*, vol. 140, no. 18, 2014.

[21] L. J. Sham and M. Schlüter, "Density-functional theory of the energy gap," *Physical Review Letters*, vol. 51, no. 20, pp. 1888–1891, 1983.

[22] P. Mori-Sánchez and A. J. Cohen, "The derivative discontinuity of the exchange-correlation functional," *Physical Chemistry Chemical Physics*, vol. 16, no. 28, pp. 14378–14387, 2014.

[23] P. Mori-Sánchez, A. J. Cohen, and W. Yang, "Localization and delocalization errors in density functional theory and implications for band-gap prediction," *Physical Review Letters*, vol. 100, no. 14, pp. 146401–146404, 2008.

[24] B. Himmetoglu, A. Floris, S. De Gironcoli, and M. Cococcioni, "Hubbard-corrected DFT energy functionals: the LDA+U description of correlated systems," *International Journal of Quantum Chemistry*, vol. 114, no. 1, pp. 14–49, 2014.

[25] W. B. Begna, G. S. Gurmesa, and C. A. Geffe, "Ortho-atomic projector assisted DFT+U study of room temperature Ferro- and antiferromagnetic Mn-doped TiO2 diluted magnetic semiconductor," *Materials Research Express*, vol. 9, no. 7, Article ID 076102, 2022.

[26] G. S. Gurmesa, N. E. Benti, M. D. Chaka et al., "Fast 3D-lithium-ion diffusion and high electronic conductivity of Li2MnSiO4surfaces for rechargeable lithium-ion batteries," *RSC Advances*, vol. 11, no. 16, pp. 9721–9730, 2021.

[27] M. K. Y. Chan and G. Ceder, "Efficient band gap prediction for solids," *Physical Review Letters*, vol. 105, no. 19, pp. 196403–196408, 2010.

[28] J. P. Perdew, W. Yang, K. Burke et al., "Understanding band gaps of solids in generalized Kohn-Sham theory," *Proceedings of the National Academy of Sciences of the United States of America*, vol. 114, no. 11, pp. 2801–2806, 2017.

[29] C. Rostgaard, K. W. Jacobsen, and K. S. Thygesen, "Fully self-consistent GW calculations for molecules," *Physical Review B*, vol. 81, no. 8, pp. 085103–085110, 2010.

[30] T. C. Li and P. Q. Tong, "Time-dependent density-functional theory for multicomponent systems," *Physical Review A*, vol. 34, no. 1, pp. 529–532, 1986.

[31] A. Dreuw, J. L. Weisman, and M. Head-Gordon, "Long-range charge-transfer excited states in time-dependent density functional theory require non-local exchange," *The Journal of Chemical Physics*, vol. 119, no. 6, pp. 2943–2946, 2003.

[32] G. S. Aga, G. S. Gurmesa, Q. Zhang, P. Singh, and C. A. Geffe, "First-principles study of the electronic and optical properties of homo-doped 2D-hBN monolayer," *Computational Condensed Matter*, vol. 30, 2022.

[33] L. Kronik, T. Stein, S. Refaely-Abramson, and R. Baer, "Excitation gaps of finite-sized systems from optimally tuned range-separated hybrid functionals," *Journal of Chemical Theory and Computation*, vol. 8, no. 5, pp. 1515–1531, 2012.

[34] T. Stein, L. Kronik, and R. Baer, "Reliable prediction of charge transfer excitations in molecular complexesusing time-dependent density functional theory," *Journal of the American Chemical Society*, vol. 131, no. 8, pp. 2818–2820, 2009.

[35] A. W. Lange, M. A. Rohrdanz, and J. M. Herbert, "Charge-transfer excited states in a π-stacked adenine dimer, as predicted using long-range-corrected time-dependent density functional theory," *The Journal of Physical Chemistry B*, vol. 112, no. 20, pp. 6304–6308, 2008.

[36] L. Hedin, "New method for calculating the one-particle Green's function with application to the electron-gas problem," *Physical Review A*, vol. 139, no. 3A, pp. A796–A823, 1965.

[37] A. Marini, G. Onida, and R. Del Sole, "Quasiparticle electronic structure of copper in theGWApproximation," *Physical Review Letters*, vol. 88, no. 1, Article ID 016403, 2001.

[38] L. Müchler, H. Zhang, and S. Chadov, "Excited states properties of organic molecules: from density functional theory to the GW and Bethe–Salpeter Green's function formalisms Excited states properties of organic molecules: from density functional theory to the GW and Bethe–salpeter Gre," *Physical Review B: Condensed Matter and Materials Physics*, vol. 7, no. 1-2, pp. 1106–1109, 2013.

[39] P. Rinke, A. Qteish, J. Neugebauer, and M. Scheffler, "Exciting prospects for solids: exact-exchange based functionals meet quasiparticle energy calculations," *Physica Status Solidi (B)*, vol. 245, no. 5, pp. 929–945, 2008.

[40] P. Rinke, A. Qteish, J. Neugebauer, C. Freysoldt, and M. Scheffler, "Combining GW calculations with exact-exchange density-functional theory: an analysis of valence-band photoemission for compound semiconductors," *New Journal of Physics*, vol. 7, 2005.

[41] X. Blase, C. Attaccalite, and V. Olevano, "First-principlesGWcalculations for fullerenes, porphyrins, phtalocyanine, and other molecules of interest for organic photovoltaic applications," *Physical Review B*, vol. 83, no. 11, pp. 115103–115109, 2011.

[42] A. L. Fetter and J. D. Walecka, "Quantum theory of many-particle systems," *Courier Corporation*, https://www.fulviofrisone.com/attachments/article/448/Fetter%20Walecka.pdf, 2021.

[43] L. Hedin and S. Lundqvist, "Effects of electron-electron and electron-phonon interactions on the one-electron states of solids," *Solid State Physics*, vol. 23, no. C, pp. 1–181, 1970.

[44] F. Aryasetiawan and O. Gunnarsson, "The GW method," *Reports on Progress in Physics*, vol. 61, no. 3, pp. 237–312, 1998.

[45] G. Onida, L. Reining, and A. Rubio, "Electronic excitations: density-functional versus many-body Green's-function approaches," *Reviews of Modern Physics*, vol. 74, no. 2, pp. 601–659, 2002.

[46] G. D. Whitfield and C. G. Kuper, "Polarons and Excitons," *Plenum Press*, https://www.ptonline.com/articles/how-to-get-better-mfi-results, 1963.

[47] Y. Lin, X. Ling, L. Yu et al., "Dielectric screening of excitons and trions in single-layer MoS2," *Nano Letters*, vol. 14, no. 10, pp. 5569–5576, 2014.

[48] A. Ramirez-Torres, V. Turkowski, and T. S. Rahman, "Time-dependent density-matrix functional theory for trion excitations: application to monolayerMoS2and other transition-metal dichalcogenides," *Physical Review B*, vol. 90, no. 8, pp. 085419–85428, 2014.

[49] I. Ozfidan, M. Korkusinski, and P. Hawrylak, "Theory of biexcitons and biexciton-exciton cascade in graphene quantum dots," *Physical Review B*, vol. 91, no. 11, pp. 115314–115319, 2015.

[50] Q. Zhang, G. Li, X. Liu et al., "A room temperature low-threshold ultraviolet plasmonic nanolaser," *Nature Communications*, vol. 5, no. 1, 2014.

[51] S. F. Chichibu, T. Azuhata, T. Sota, and T. Mukai, "Localized excitons in an In0.06Ga0.94N multiple-quantum-well laser diode lased at 400 nm," *Applied Physics Letters*, vol. 79, no. 3, pp. 341–343, 2001.

[52] E. Collado-Fregoso, P. Boufflet, Z. Fei et al., "Increased exciton dipole moment translates into charge-transfer excitons in thiophene-fluorinated low-bandgap polymers for organic photovoltaic applications," *Chemistry of Materials*, vol. 27, no. 23, pp. 7934–7944, 2015.

[53] P. Giannozzi, S. Baroni, N. Bonini et al., "Quantum espresso: a modular and open-source software project for quantum simulations of materials," *Journal of Physics: Condensed Matter*, vol. 21, no. 39, Article ID 395502, 2009.

[54] P. Giannozzi, O. Andreussi, T. Brumme et al., "Advanced capabilities for materials modelling with Quantum ESPRESSO," *Journal of Physics: Condensed Matter*, vol. 29, no. 46, Article ID 465901, 2017.

[55] J. P. Perdew, K. Burke, and M. Ernzerhof, "Generalized gradient approximation made simple," *Physical Review Letters*, vol. 77, no. 18, pp. 3865–3868, 1996.

[56] J. W. Song, K. Yamashita, and K. Hirao, "Communication: a new hybrid exchange correlation functional for band-gap calculations using a short-range Gaussian attenuation (Gaussian-Perdue-Burke- Ernzerhof)," *The Journal of Chemical Physics*, vol. 135, no. 7, Article ID 071103, 2011.

[57] D. R. Hamann, "Optimized norm-conserving Vanderbilt pseudopotentials," *Physical Review B*, vol. 88, no. 8, pp. 085117–85210, 2013.

[58] T. H. Fischer and J. Almlöf, "General methods for geometry and wave function optimization," *Journal of Physical Chemistry*, vol. 96, no. 24, pp. 9768–9774, 1992.

[59] D. Nabok, A. Gulans, and C. Draxl, "Accurate all-electronG0W0quasiparticle energies employing the full-potential augmented plane-wave method," *Physical Review B: Condensed Matter*, vol. 94, no. 3, pp. 035118-035119, 2016.

[60] A. Marini, C. Hogan, M. Grüning, and D. Varsano, "yambo: an ab initio tool for excited state calculations," *Computer Physics Communications*, vol. 180, no. 8, pp. 1392–1403, 2009.

[61] D. Sangalli, A. Ferretti, H. Miranda et al., "Many-body perturbation theory calculations using the yambo code," *Journal of Physics: Condensed Matter*, vol. 31, no. 32, Article ID 325902, 2019.

[62] P. Larson, M. Dvorak, and Z. Wu, "Role of the plasmon-pole model in theGWapproximation," *Physical Review B*, vol. 88, no. 12, pp. 125205–125246, 2013.

[63] R. W. Godby and R. J. Needs, "Metal-insulator transition in Kohn-Sham theory and quasiparticle theory," *Physical Review Letters*, vol. 62, no. 10, pp. 1169–1172, 1989.

[64] M. Strange and K. S. Thygesen, "Image-charge-induced localization of molecular orbitals at metal-molecule interfaces: self-consistentGWcalculations," *Physical Review B*, vol. 86, no. 19, pp. 195121–195126, 2012.

[65] G. Strinati, "Effects of dynamical screening on resonances at inner-shell thresholds in semiconductors," *Physical Review B: Condensed Matter*, vol. 29, no. 10, pp. 5718–5726, 1984.

[66] M. Rohlfing and S. G. Louie, "Electron-hole excitations and optical spectra from first principles," *Physical Review B: Condensed Matter*, vol. 62, no. 8, pp. 4927–4944, 2000.

[67] M. Palummo, O. Pulci, R. D. Sole et al., "The Bethe-Salpeter equation: a first-principles approach for calculating surface optical spectra," *Journal of Physics: Condensed Matter*, vol. 16, no. 39, pp. S4313–S4322, 2004.

[68] A. Molina-Sánchez, D. Sangalli, K. Hummer, A. Marini, and L. Wirtz, "Effect of spin-orbit interaction on the optical spectra of single-layer, double-layer, and bulk MoS2," *Physical Review B*, vol. 88, no. 4, pp. 045412–045416, 2013.

[69] M. Cardona, L. F. Lastras-Martínez, and D. E. Aspnes, "Comment on Ab initio calculation of excitonic effects in the optical spectra of semiconductors," *Physical Review Letters*, vol. 83, no. 19, 1999.

[70] L. X. Benedict, E. L. Shirley, and R. B. Bohn, "Optical absorption of insulators and the electron-hole interaction: an ab initio calculation," *Physical Review Letters*, vol. 80, no. 20, pp. 4514–4517, 1998.

[71] G. Strinati, "Application of the Green's functions method to the study of the optical properties of semiconductors," *La Rivista del Nuovo Cimento*, vol. 11, no. 12, pp. 1–86, 1988.

[72] M. Shahrokhi and C. Leonard, "Tuning the band gap and optical spectra of silicon-doped graphene: many-body effects and excitonic states," *Journal of Alloys and Compounds*, vol. 693, pp. 1185–1196, 2017.

[73] M. Van Schilfgaarde, T. Kotani, and S. Faleev, "Quasiparticle self-ConsistentGWTheory," *Physical Review Letters*, vol. 96, no. 22, pp. 226402–226404, 2006.

[74] M. Shishkin and G. Kresse, "Self-consistentGWcalculations for semiconductors and insulators," *Physical Review B*, vol. 75, no. 23, pp. 235102–235109, 2007.

[75] S. Y. Bao, F. S. Liu, B. Tang, Q. J. Liu, C. L. Jiang, and X. J. Ma, "Phonon, electronic structure and mechanical properties of superhard material BC2N from first-principles calculations," *Brazilian Journal of Physics*, vol. 51, no. 4, pp. 1199–1206, 2021.

[76] S. Sharifzadeh, A. Biller, L. Kronik, and J. B. Neaton, "Quasiparticle and optical spectroscopy of the organic semiconductors pentacene and PTCDA from first principles," *Physical Review B*, vol. 85, no. 12, pp. 125307–125311, 2012.

[77] S. Sharifzadeh, P. Darancet, L. Kronik, and J. B. Neaton, "Low-energy charge-transfer excitons in organic solids from first-principles: the case of pentacene," *Journal of Physical Chemistry Letters*, vol. 4, no. 13, pp. 2197–2201, 2013.